

Article

Composites of Layered Double Hydroxides and ANA-Type Zeolite Synthesized from Hazardous Secondary Aluminum Dross for Cationic Dye Wastewater Treatment

Bin Zhu ^{1,*}, Lina Wang ², Guo Li ² and Qiang Jin ¹¹ School of Environmental Science and Engineering, Shanghai Jiao Tong University, Shanghai 200240, China² China Communications Construction Sinobioway Environmental Protection Co., Ltd., Jinan 250000, China

* Correspondence: zhubin912@sjtu.edu.cn; Tel.: +81-021-54741065

Abstract: This work first transformed hazardous aluminum waste into low-cost MgAl-layered double hydroxide@ANA zeolite (LDHs@ANA) composite for dye wastewater adsorption, which was meaningful for waste recovery and pollution control. Based on this strategy, the Al(OH)₃ extracted from secondary aluminum dross (a hazardous waste in the aluminum industry) was used as an aluminum source to synthesize LDHs@ANA composite, which had more excellent adsorption capacity to methylene blue than MgAl-LDHs and ANA alone. The composite consisted of spherical ANA particles uniformly covered with LDH nanosheets, which effectively avoided a large amount of aggregation between nanosheets and increased specific surface areas and pore volumes. The kinetic results indicated that the adsorption process conformed to the pseudo-second-order kinetic model, and the adsorption site was the main factor affecting the adsorption process. The equilibrium studies showed the adsorption process was exothermic, and the Langmuir model best fitted for the adsorption process, with a maximum adsorption capacity reaching 65.27 mg/g. Meanwhile, the effects of pH, adsorbent concentration, initial methylene blue concentration, and adsorption time on the LDHs@ANA were analyzed. Overall, this work provides a fresh concept for the preparation of low-cost adsorbents from aluminum waste.



Citation: Zhu, B.; Wang, L.; Li, G.; Jin, Q. Composites of Layered Double Hydroxides and ANA-Type Zeolite Synthesized from Hazardous Secondary Aluminum Dross for Cationic Dye Wastewater Treatment. *Processes* **2023**, *11*, 1002. <https://doi.org/10.3390/pr11041002>

Academic Editors: Marcin Banach, Olga Długosz and Jolanta Pulit-Prociak

Received: 22 February 2023

Revised: 16 March 2023

Accepted: 24 March 2023

Published: 26 March 2023



Copyright: © 2023 by the authors. Licensee MDPI, Basel, Switzerland. This article is an open access article distributed under the terms and conditions of the Creative Commons Attribution (CC BY) license (<https://creativecommons.org/licenses/by/4.0/>).

Keywords: secondary aluminum dross; layered double hydroxides; zeolites; composite material; dye adsorption

1. Introduction

Secondary aluminum dross (SAD) is a typical and unavoidable waste in the aluminum industry, with an annual global production of more than 1 million tons [1]. Depending on the scrap source, SAD usually contains 20–60 wt% α -alumina, 5–10 wt% aluminum, 5–50 wt% salt flux (NaCl, KCl and fluoride salts, etc.), and other minor impurities [2,3]. Usually, 95% of the SAD was directly landfilled [4]. In recent years, most countries have classified SAD as hazardous waste and banned its direct landfill due to its high reactivity, leachability, and toxicity [5]. Meanwhile, SAD is rich in aluminum resources with a high recovery value, even 5–30% higher than bauxite. Various treatment technologies, such as sintering [6], acid leaching [7], and alkali leaching [8], have focused on the recovery of alumina and aluminum resources. However, the high-value utilization of SAD is extremely inefficient, causing vast resource waste. In order to solve the environmental pollution risk and waste of aluminum resources in SAD, the development of a high-value-added SAD recovery process is highly pursued and urgent.

On the other hand, as a synthetic cationic dye, methylene blue (MB) is widely used in the printing and dyeing industry [9,10]. Meanwhile, MB is toxic, environmentally persistent, non-biodegradable, and can also produce carcinogenic and mutagenic components through reductive anaerobic degradation [11]. The discharge of MB into water can cause serious harm to aquatic plants, aquatic animals, and even the ecosystems throughout the

food chain [12]. Therefore, it is crucial to effectively remove MB from the aqueous environment. Typical MB removal methods include adsorption [13,14], bioremediation [15,16], advanced oxidation [17], etc. Among these methods, adsorption is the most commonly used technique, which has the advantages of high efficiency, easy operation, and no secondary pollution [18,19].

Layered double hydroxides (LDHs) are a widely used class of anionic clay with the general formula of $[M_{1-x}^{2+}M_x^{3+}(\text{OH})_2](A^{n-})_{x/n} \cdot y\text{H}_2\text{O}$ (where M^{2+} and M^{3+} are divalent and trivalent metals) [20,21]. In recent years, due to the potential layered structure, multi-level pore structure, and excellent anion exchange capacity [22], LDHs have shown excellent adsorption and removal ability for many anionic dyes such as congo red [23], methyl orange [24], acid red GR [25], Evans blue [26], and Acid brown 14 [27], etc. However, the positively charged hydrotalcite-like host layer of LDHs limits the incorporation of cationic dyes. Most of the previously reported LDHs exhibit poor cationic dye adsorption performance [28,29]. Finding a modification method to increase the combination between LDHs and cationic dyes is of great significance for improving the adsorption capacity of LDHs to MB.

Zeolites are aluminum–silicate crystalline microporous compounds with internal channels capable of easily exchangeable cations [30]. Due to their high adsorption capacity, good selectivity, and thermal stability, zeolites are widely used in sewage purification [31], gas separation [32], and other related fields. Furthermore, due to their structural versatility and diversity, zeolites are regarded as suitably modified substrates for shell@core structure composites [33]. Li et al. [33] prepared MgAl–LDHs and natural zeolite composites for rapid co-adsorption of NH_4^+ and NO_3^- . Wu et al. [34] prepared Ca/Fe-LDHs and natural zeolite composites to effectively reduce the risk of sediment-P release. Therefore, analcime type zeolite (ANA) was selected as the modified matrix material for LDHs. The introduction of ANA reversed the surface charge properties of LDHs and enhanced the binding of LDHs to cationic dyes. The two-dimensional LDHs grown on the three-dimensional ANA provided more adsorption sites for LDHs and facilitated the recovery of hydrophilic nano-LDHs. In addition, in order to simultaneously solve the problem of hazardous SAD recovery and reduce the cost of composites, MgAl–LDH was selected as the loading material, and SAD was used as the aluminum source to synthesize LDHs@ANA composites. The beneficiation of aluminum waste into sorbents that can be utilized to eliminate contaminants from water systems is poorly studied. The potential advantage of the composite is the ability to accomplish dual benefits of waste treatment and environmental remediation in comparison to other adsorbents (such as commercial activated carbon).

In this study, firstly, we used acid leaching and alkali purification methods to extract aluminum elements from hazardous SAD. Then, a novel composite was prepared with MgAl–LDHs uniformly grown on analcime zeolite (ANA) using SAD as an aluminum source by a one-step hydrothermal method. Finally, we successfully applied LDHs@ANA composite to the adsorption of MB in dye wastewater. The LDHs@ANA composite was characterized by various structural analysis techniques. Then the effects of pH, adsorbent concentration, initial methylene blue (MB) concentration, and adsorption time on the LDHs@ANA composite were analyzed, and the adsorption kinetic and equilibrium isotherm were analyzed. This work first transformed hazardous aluminum waste into LDHs@ANA for dye wastewater adsorption, which was meaningful to waste recovery and pollution control.

2. Materials and Methods

2.1. Materials and Reagents

The SAD used herein was provided by Jiangsu Haiguang Co., Ltd., Suqian, Jiangsu, China, which was devoted to secondary aluminum remelting and smelting. Previous studies showed that aluminum extraction from SAD by acid leaching resulted in a higher extraction efficiency than alkaline leaching [8]. Thus, an acid extraction method was chosen

in this study to obtain more aluminum. After adequate grinding and washing, the SAD was filtered and dried in an oven for subsequent use. The leaching experiments were performed in a conical flask equipped with reflux condensers. SAD (6 g) was taken into 60 mL HCl solution (1 mol/L to 6 mol/L) with 10 mL/g, and then kept at a temperature of 85 °C and a stirring speed of 600 r/min for 2 h. The leachate was further purified and dried with alkali, and the detailed method was reported in the published literature [1,35].

MgCl₂·6H₂O, NaOH, HCl, urea, NH₃·H₂O and Na₂SiO₃, and MB were purchased from Sinopharm Chemical Reagent Co., Ltd. (Shanghai, China). All chemical reagents were analytical-grade.

2.2. Preparation of LDH@zeolite Composites

2.2.1. Synthesis of Zeolite

The ANA was prepared by a conventional hydrothermal method without prior activation steps and without the use of organic templates. Al(OH)₃ extracted from SAD, NaOH, and H₂O were placed into a Teflon-lined container and dissolved by ultrasound completely. Then, ultrasonically dissolved Na₂SiO₃ solution was added to the above mixture (n(Na₂O): n(SiO₂): n(Al₂O₃): n(H₂O) = 1.66:1:0.19:116). After mixing thoroughly, the solution was held in a 100 mL Teflon-lined stainless-steel autoclave and heated in an oven to 150 °C for 6 h. After cooling, the prepared zeolite was washed with H₂O and C₂H₅OH and dried at a temperature of 80 °C for 6 h.

2.2.2. Synthesis of MgAl-LDHs and LDHs@ANA Composite

The synthesis of MgAl-LDHs was performed by the hydrothermal method. Specifically, 20 mL deionized water, 2.5 mmol Al(OH)₃ extracted from SAD, and 18.8 mmol urea were mixed with a certain amount of MgCl₂·6H₂O, which was calculated according to the Mg/Al molar ratio varied from 4:1 to 2:1. The homogeneous mixture was then transferred into a Teflon-lined autoclave and heated at 150 °C for 6 h. The sample was filtered and washed to neutral pH with deionized water, then dried at 80 °C for 6 h.

The LDHs@ANA was synthesized by procedures and conditions similar to MgAl-LDHs. Specifically, 20 mL deionized water, 2.5 mmol Al(OH)₃ extracted from SAD, 5 mmol MgCl₂·6H₂O, and 18.8 mmol urea were mixed with corresponding ANA, which was calculated according to the MgAl-LDHs: ANA mass ratio was about 1:2. The homogeneous mixture was then transferred into a Teflon-lined autoclave and heated at 150 °C for 6 h. The sample was filtered and washed to neutral pH with deionized water, then dried at 80 °C for 6 h. Overall, the ANA, MgAl-LDHs, and LDHs@ANA were synthesized as shown in Figure 1.

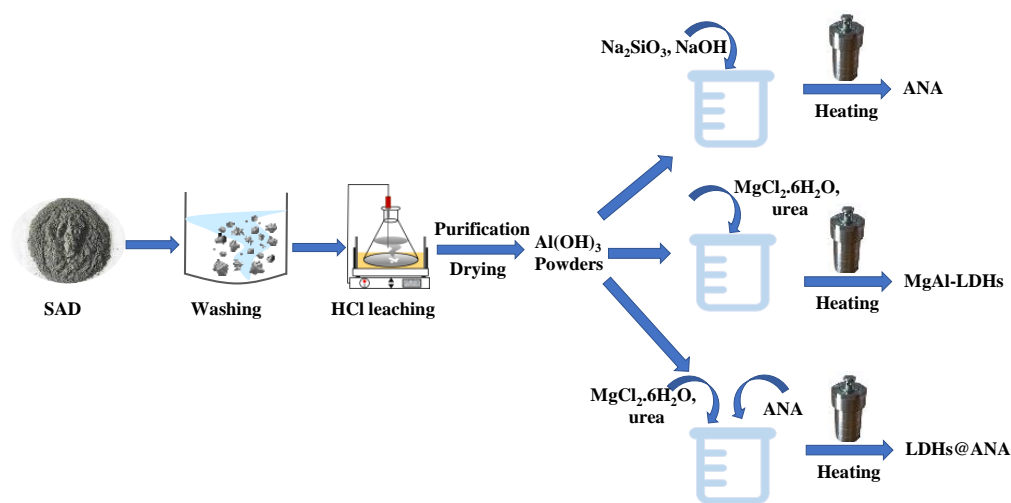


Figure 1. The fabrication process of the preparation of ANA, MgAl-LDHs, and LDHs@ANA.

2.3. Batch Experiments and Adsorption Kinetics

A series of 100 mL water samples were prepared with MB concentrations of 20, 50, and 100 mg/L. The effects of pH, adsorbent concentration, initial methylene blue (MB) concentration, and adsorption time on the LDHs@ANA composite were analyzed. The initial pH was adjusted by dilute HCl or NaOH, and the pH was measured with a pH meter. The MB concentrations of pollutants in the solution were determined by UV-Vis spectrophotometry (UV-Vis; SP-756PC, Shanghai, China). The detection wavelength of MB is 665 nm. All samples were diluted five times before measurement.

The degradation experiment was carried out in a 250 mL Erlenmeyer flask, and the Erlenmeyer flask was shaken at 200 r/min in an incubator (constant temperature oscillator) at the temperature of 20 °C. A total of 5 mL of the solution from the Erlenmeyer flask was taken at specific reaction times (0.5, 1, 3, 5, 10, 20, 30, 45, and 60 min) and filtered through a 0.22 µm filter. The adsorbent dosage and the initial pH were 3 g/L and 7, respectively. The adsorption kinetics of MB were fitted by pseudo-first-order and pseudo-second-order kinetic models (Equations (1) and (2)), respectively [36].

$$q_t = q_e(1 - \exp(-k_m t)) \quad (1)$$

$$q_t = \frac{k_n q_e^2 t}{1 + k_n q_e t} \quad (2)$$

where q_t and q_e are adsorption capacity (mg/g) of MB at moment t and equilibrium (min), respectively. k_m (min^{-1}), k_n ($\text{g}/(\text{mg}\cdot\text{min})$) are the rate constants of the pseudo-first-order kinetics model, and pseudo-second-order kinetics model.

2.4. Equilibrium Isotherm

A series of 100 mL water samples were prepared with MB concentration from 40 mg/L to 300 mg/L. The adsorption capacity at different temperatures (20 °C, 30 °C, and 40 °C) was investigated after adsorption for 120 min. The adsorbent dosage and the initial pH value were 3 g/L and 7, respectively. After the reaction, the residual MB was measured after filtering through a 0.22 µm filter membrane. The experimental data were fitted by Langmuir, Freundlich, and Temkin (Equations (3)–(5) [33]) adsorption isotherm models, respectively.

$$q_e = q_m \frac{k_L C_e}{1 + k_L C_e} \quad (3)$$

$$q_e = k_F C_e^{\frac{1}{n}} \quad (4)$$

$$q_e = B_T \ln(k_T C_e) \quad (5)$$

where q_e and C_e are the adsorption capacity (mg/g) and equilibrium concentration (mg/L) of MB, respectively. k_L (L/mmol) is the Langmuir constant, which is related to the number of adsorption sites per unit mass of adsorbent, k_F ($\text{mg}\cdot\text{g}\cdot(\text{L}/\text{mg})^{1/n}$) and n is the Freundlich constants related to adsorption capacity and adsorption intensity, respectively, the B_T and k_T are constants related to the maximum binding energy and average binding energy, respectively.

2.5. Characterization Method

Elemental analysis of the SAD sample and as-synthesized $\text{Al}(\text{OH})_3$ powders from SAD was performed using a wavelength-dispersive X-ray fluorescence spectrometer (XRF, XRF1800, Shimadzu Co. Ltd., Kyoto, Japan). The Al content in the leaching solution and metallic concentration of synthetic materials were determined by an Inductively Coupled Plasma Optical Emission Spectrometer (ICP–OES) analyzer (PerkinElmer Ltd., Waltham, MA, USA). The crystalline structure of the samples was determined by X-ray diffractometer

(XRD, XRD-6100, Shimadzu Co., Ltd., Kyoto, Japan; scanning rate $2.0^\circ \text{ min}^{-1}$, scanning range $5\text{--}80^\circ$ (2θ), step 0.02). The morphology and corresponding elemental composition were characterized by high-resolution field emission scanning electron microscopy (SEM, JSM-7800F, JEOL Ltd., Akishima-shi, Tokyo, Japan) with electron dispersive spectroscopy (EDS). The N_2 adsorption-desorption experiments were carried out by using a surface area analyzer (ASAP 2460, Micromeritics, Norcross, GA, USA) at 77.3 K, and the specific surface area and pore size distribution were analyzed by Brunauer–Emmett–Teller (BET) and Barrett–Joyner–Halenda (BJH) methods. The Fourier transform infrared (FT-IR) spectra were generated on a Fourier transform infrared spectrometer (Thermo Fisher Scientific Inc., MA, USA) with the range of $400\text{--}4000 \text{ cm}^{-1}$.

3. Results

3.1. Extraction of Aluminum Elements from SAD

3.1.1. Characterization of Raw SAD

The chemical analysis and XRD analysis are detailed in Table 1 and Figure 2, respectively. The high proportion of Al element (48.63 wt%) indicated that SAD is a high-alumina material, which has the potential to be reformed into an effective aluminum-containing wastewater treatment material. Among them, the aluminum elements are mainly composed of alpha-alumina, spinel, AlN, and Al. Furthermore, small amounts of soluble salts (Na, K, F, Cl) and alloy elements (Fe, Mg, Si) were present in SAD. Due to the complex composition of SAD, the separation of aluminum elements in SAD is challenging.

Table 1. Chemical analysis of raw SAD samples.

Element	Contents (%)	Element	Contents (%)
Al	48.63	Cu	0.74
O	21.32	Ti	0.63
Mg	4.55	Mn	0.54
Fe	3.69	Zn	0.37
Si	3.31	Cr	0.19
Cl	2.88	Ba	0.43
F	2.25	S	0.11
Ca	1.62	Sr	0.04
Na	1.19	Ni	0.02
K	0.79	-	-

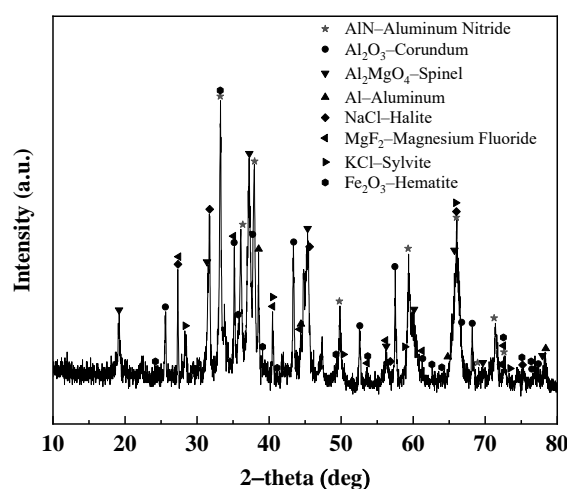


Figure 2. XRD spectra of raw SAD.

3.1.2. Extraction of Aluminum from SAD

Soluble salts in SAD must be removed to avoid interference with zeolite and MgAl-LDHs synthesis [37]. Therefore, grinding and washing pretreatment to recover soluble salts were

necessary. After pretreatment, as shown in Figure 3a, the AlN and Al phases in SAD almost disappeared and transformed into boehmite, and the soluble salts were also separated by washing. After grinding and washing pretreatment, HCl was chosen as a leaching reagent for aluminum extraction. The extraction rate of aluminum in SAD with different concentrations of HCl was investigated (Figure 3b). As the concentration of HCl increased from 1 mol/L to 6 mol/L, the leaching rate of aluminum in SAD increased from 23.2% to 90.7%. Considering the leaching effect, 6 mol/L HCl was chosen for the extraction of aluminum elements from SAD, and the corresponding extraction efficiency of aluminum reached 90.7%. After the 6 mol/L HCl acid treatment, the residues were mainly insoluble spinel and corundum (Figure 3a). After leaching, the leachate was further purified and dried using alkali [1,35], and the composition and content of the obtained $\text{Al}(\text{OH})_3$ are shown in Table 2.

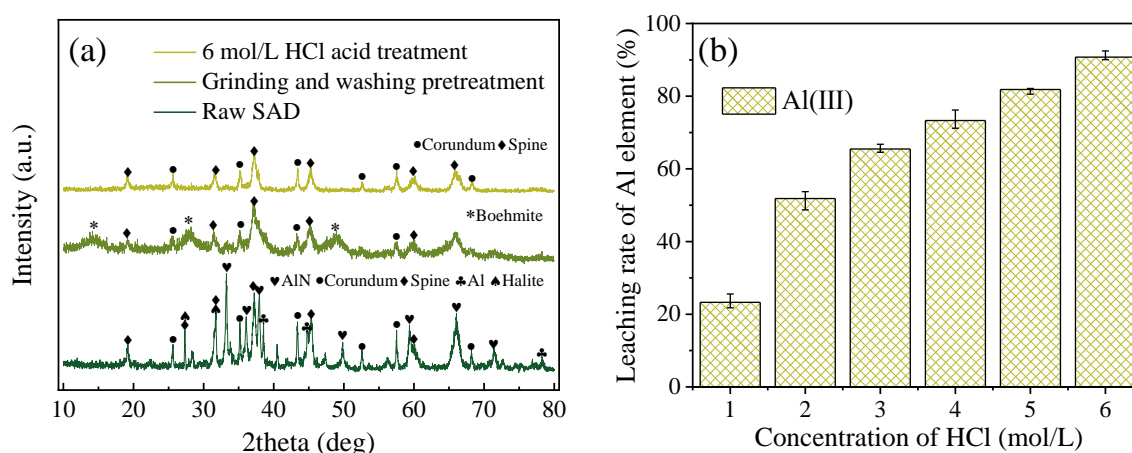


Figure 3. (a) XRD patterns of SAD before and after HCl leaching; (b) leaching rate of Al element by different concentrations of HCl.

Table 2. XRF analysis of as-synthesized $\text{Al}(\text{OH})_3$ powders from SAD.

Oxide	Al_2O_3	Na_2O	SiO_2	Fe_2O_3	CaO	ZnO	CuO
Content (wt.%)	94.58	1.87	1.19	1.16	0.77	0.24	0.17

3.2. Structure of Synthetic Mg/Al-LDHs, Zeolite, and LDHs@zeolite Composites

3.2.1. Characterization of Mg/Al-LDHs and Zeolite

The crystal phases of Mg/Al-LDHs and zeolite were characterized by XRD analysis (Figure 4). As presented in Figure 4a, the characteristic diffraction peaks observed at 2θ values of 11.7° , 23.4° , 34.9° , 39.4° , and 46.9° of Mg/Al-LDHs (with different Mg: Al molar ratios from 2 to 4) corresponded to the (003), (006), (0012), (0015), and (0018) crystal planes, respectively. The typical characteristic diffraction peaks could be indexed to the Mg/Al-LDHs with a typical layered structure of carbonate layered hydroxide (PDF#01-89-0460). Although the sharp experimental XRD diffraction peak indicated good crystallinity of all samples, the Mg_2Al -LDHs had the highest peak height and no impurity peaks. Therefore, Mg_2Al -LDHs were chosen for subsequent composite synthesis. Murayama et al. [38] used aluminum dross as an aluminum source to prepare Mg/Al-LDHs, and found that some unidentified peaks existed in the products, indicating that the product was relatively impure. In our case, the LDHs were obtained directly from the transformation of the aluminum waste and had high purity and crystallinity.

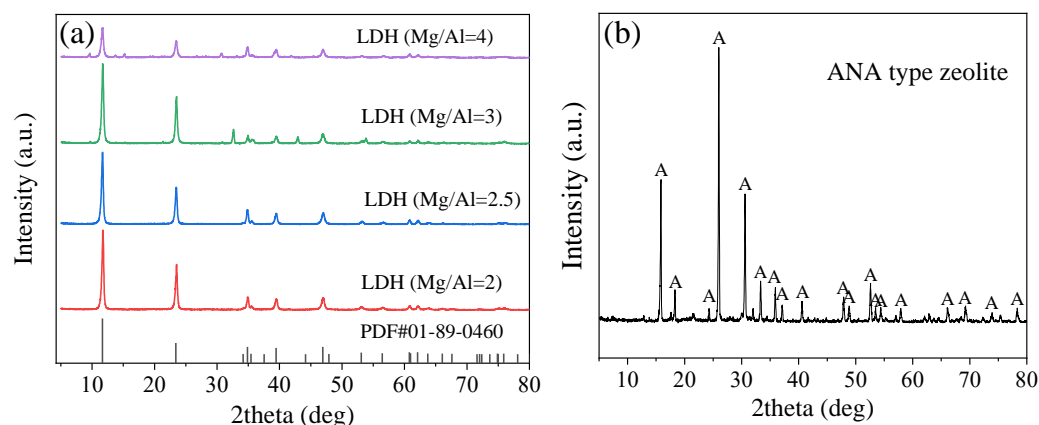


Figure 4. (a) XRD patterns of LDHs with different Mg/Al ratio, (b) XRD patterns of ANA.

For the synthetic zeolite, the XRD pattern (Figure 4b) indicated the analcime (PDF# 00-041-1478) was the only phase with high purity and crystallinity. The sharp shape indicated the high crystallinity of the synthetic analcime (ANA). ANA is usually obtained by long-term reactions at high temperatures. In this study, the ANA was obtained within a short time (6 h) at 150 °C in agreement with the study of Sánchez–Hernández et al. [39].

3.2.2. Characterization of LDHs@zeolite Composites

In the XRD patterns of LDHs@zeolite composites (Figure 5a), the diffraction peaks of 15.8°, 26.0°, 30.6°, and 33.3° corresponded to (211), (400), (332), and (431) crystal planes of ANA (PDF# 00-041-1478), respectively. Meanwhile, the diffraction peaks of 11.7°, 23.4°, and 34.9° corresponded to (003), (006), and (012) crystal planes of MgAl–LDHs (PDF#01-89-0460), respectively. The XRD images indicated that MgAl–LDHs were successfully loaded onto ANA. Compared with MgAl–LDHs and ANA alone, the peak height of the LDHs@ANA was reduced. This may be due to the lattice distortion caused by the addition of ANA during the preparation of MgAl–LDHs, which demonstrated the successful preparation of the LDHs@ANA composites.

Figure 5b shows the FTIR spectrums of MgAl–LDHs, ANA, and LDHs@ANA. The broadband near 3436 cm^{-1} was attributed to the stretching vibration of O–H bonds [40]. The stretching vibration bands of CO_3^{2-} appeared around 1356 cm^{-1} and were relatively sharp [41] because CO_2 produced by hydrolysis of urea was dissolved in the water and inserted into the interlayer of MgAl–LDHs in the form of CO_3^{2-} . The intensity of the absorption band near 991 cm^{-1} was produced by the stretching vibration of Si–O [42]. The absorption bands of MgAl–LDH and ANA appeared simultaneously in the FTIR spectra of the composites, indicating the successful preparation of LDHs@ANA composites.

The specific surface area of ANA, LDHs, and LDHs@ANA composites was analyzed by the N_2 adsorption–desorption isotherms (Figure 5c). As seen in Figure 5c, the adsorption isotherms of LDHs and LDHs@ANA belonged to type IV isotherm with H3-type hysteresis loop [43], indicating the presence of mesoporous structures in LDHs@ANA. Table 3 shows the S_{BET} of ANA, LDHs, and LDHs@ANA were 27.4, 30.2, and 60.8 $\text{m}^2 \cdot \text{g}^{-1}$, respectively. The specific surface area of the composite material was the largest, more than double that of LDHs and ANA alone. Due to the addition of ANA, the LDHs had more ordered growth and effectively reduced the overlap and aggregation of nanosheets, leading to a more uniform and smaller pore size (Figure 5d). The increased specific surface area could enhance the contact between the composite and MB and improve the adsorption efficiency of MB.

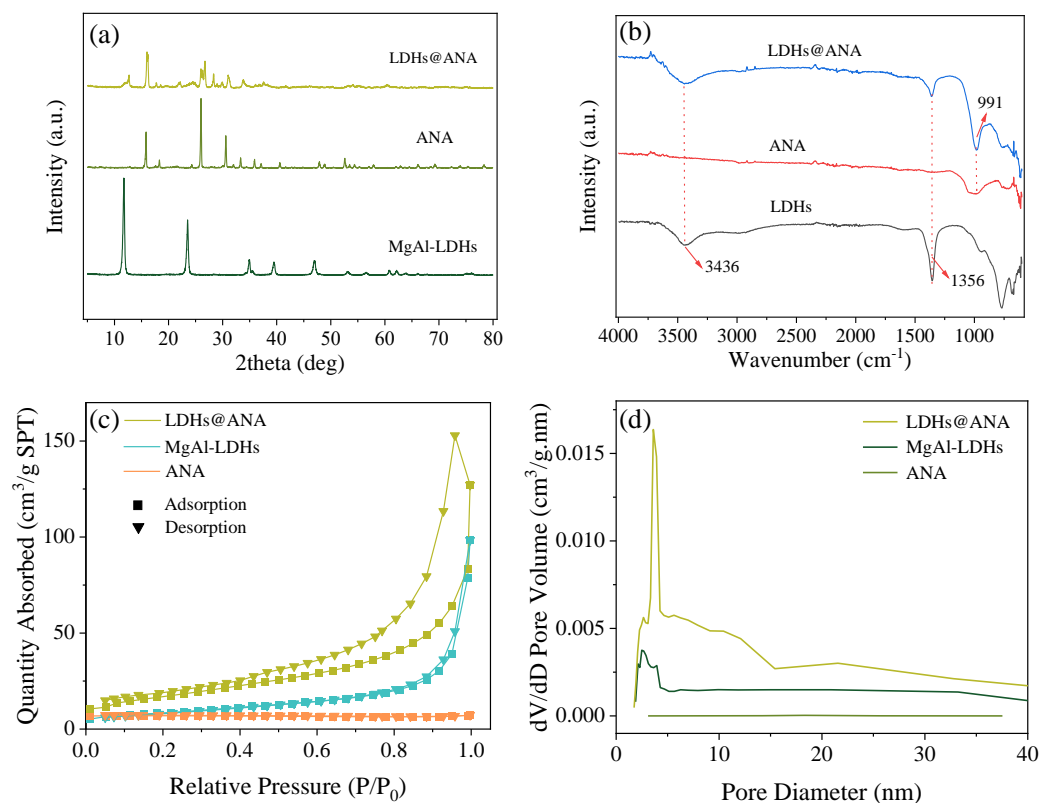


Figure 5. MgAl-LDHs, ANA, and LDHs@ANA of (a) XRD patterns, (b) FT-IR spectra, (c) N₂ adsorption-desorption isotherm curves, and (d) pore size distribution.

Table 3. N₂ adsorption-desorption characteristics of ANA, MgAl-LDHs, and LDHs@ANA.

	S _{BET} (m ² /g)	V _{pore} (cm ³ /g)	D _{BJH} (nm)
ANA	27.4	0.011	30.4
MgAl-LDHs	30.2	0.15	19.8
LDHs@ANA	60.8	0.24	13.8

S_{BET}: BET surface area; V_{pore}: total pore volume (pore diameter < 667.9 nm, P/P₀ = 0.9971); D_{BJH}: BJH desorption average pore diameter (4V/A).

LDHs, ANA, and LDHs@ANA composites were prepared by hydrothermal method, and their SEM-EDS are shown in Figure 5. MgAl-LDHs (Figure 6a) consisted of disordered stacks of irregular nanosheets with a thickness of about 40 nm. The EDS image showed that MgAl-LDHs were mainly composed of C, O, Mg, Al, and the Mg/Al atomic ratio was 2.1, consistent with the XRD results. In addition, a small amount of Si was present, which was the impurity during the extraction of Al by SAD. ANA (Figure 6b) consisted of uniform and independent spherical particles with a diameter of about 20–60 μm. The individual particles could be observed as highly polyhedral pentagonal crystals with sharp edges. Furthermore, the EDS image showed that ANA was composed of Si, Al, O, and Na, where the Si/Al atomic ratio was 2.5. As shown in Figure 6c, the LDHs@ANA composite consisted of spherical ANA particles uniformly covered with MgAl-LDHs nanosheets. MgAl-LDHs were anchored and grown on the surface of ANA, effectively avoiding a large amount of aggregation between nanosheets. Therefore, the utilization efficiency of MgAl-LDHs was improved by the introduction of ANA and could provide more active sites for MB adsorption.

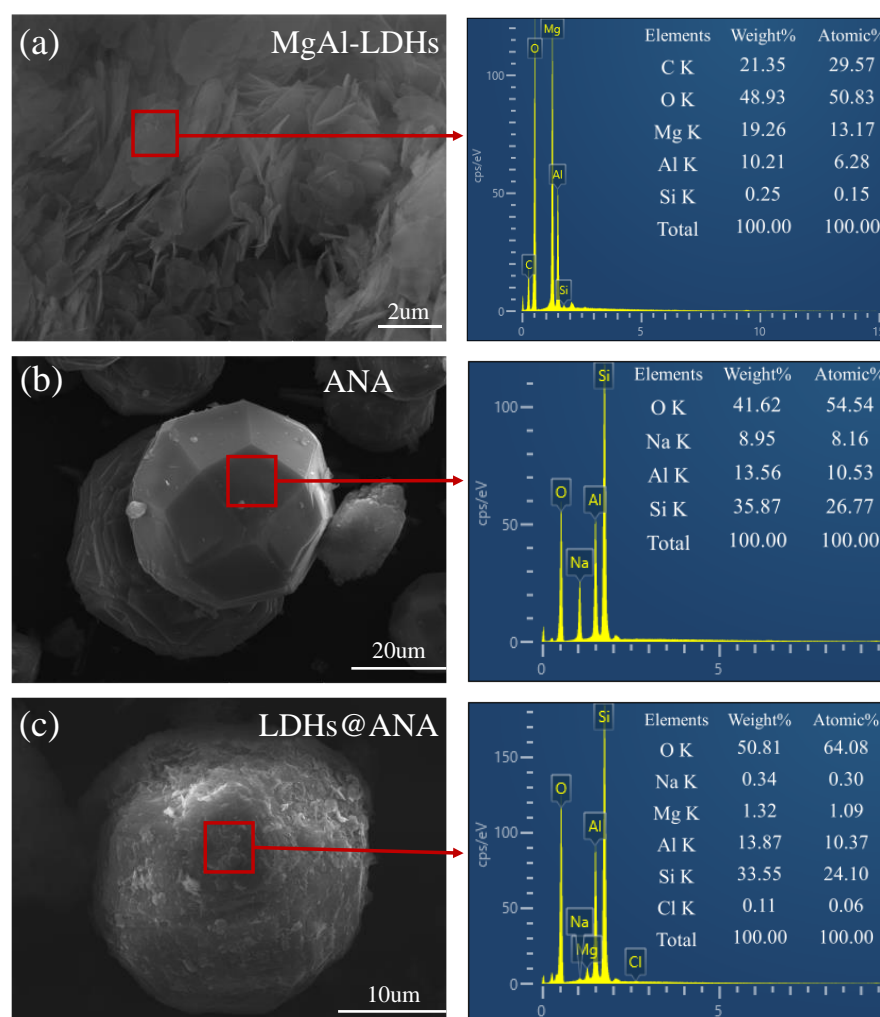


Figure 6. SEM images and EDS spectra of (a) MgAl-LDHs, (b) ANA, and (c) LDHs@ANA.

Notably, compared with MgAl-LDHs, no carbon element was observed in the LDHs@ANA composite in the EDS analysis. To further determine the chemical composition of LDHs@ANA, the ICP analysis of metal elements and XPS analysis of C1s in MgAl-LDHs and LDHs@ANA were analyzed, as shown in Table S1 and Figure 7. As seen in Figure 7, the C1s spectrum of LDHs@ANA consisted of C-C, C-O, and C=O bonds at 284.9, 286.6, and 288.9 eV, respectively. Furthermore, the C1s spectrum of MgAl-LDHs consisted of 284.8, 286.4, and 288.7 eV, respectively. The C-O and C=O of MgAl-LDHs and LDHs@ANA belonged to CO_3^{2-} of LDHs. Compared with LDHs, all peaks of the C1s spectrum in LDHs@ANA showed a slightly positive deviation. The shift in binding energy was due to the interaction between the cations of LDH nanosheets and the oxygen-containing groups of ANA [44]. Furthermore, compared with LDHs, the vibration band of CO_3^{2-} in the FT-IR spectrum in LDHs@ANA weakened (Figure 5b). This may be because the LDHs have undergone a process of exfoliation, and the brucite-like lamellae cover the zeolite, which led to the collapse of the lamellar structure, eliminating the part interlamellar anion of CO_3^{2-} .

3.3. Factors Affecting MB Adsorption

3.3.1. Effect of Adsorbent Concentration on MB Adsorption

Figure 8a shows the effect of LDHs@ANA adsorbent doses on the adsorption of MB. The MB adsorption efficiency increased with the increase in the adsorbent dosage. Specifically, when the dosage of LDHs@ANA increased from 0.4 to $5 \text{ g} \cdot \text{L}^{-1}$, the Re values increased obviously from 45.8% to 99.9%, while the Qe decreased from $22.9 \text{ mg} \cdot \text{g}^{-1}$ to

$4.0 \text{ mg}\cdot\text{g}^{-1}$. With the increase of adsorbent, the adsorption sites were increased, and more MB was adsorbed, thus increasing the Re. At the same time, it led to an increase in the length of the diffusion path and a decrease in the surface area in the case of higher aggregation of the particles, thus reducing the Qe. When the LDHs@ANA adsorbent dose concentration was 5 g/L , the Re of MB reached 99.9%, which meant MB was almost adsorbed. Therefore, the adsorbent dosage for subsequent experiments was chosen to be 3 g/L .

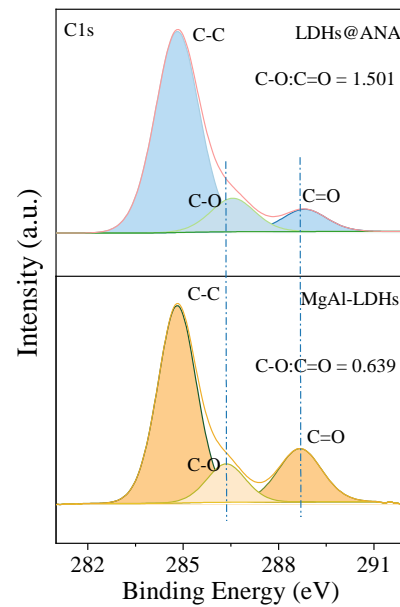


Figure 7. XPS spectra of C1s in MgAl-LDHs and LDHs@ANA.

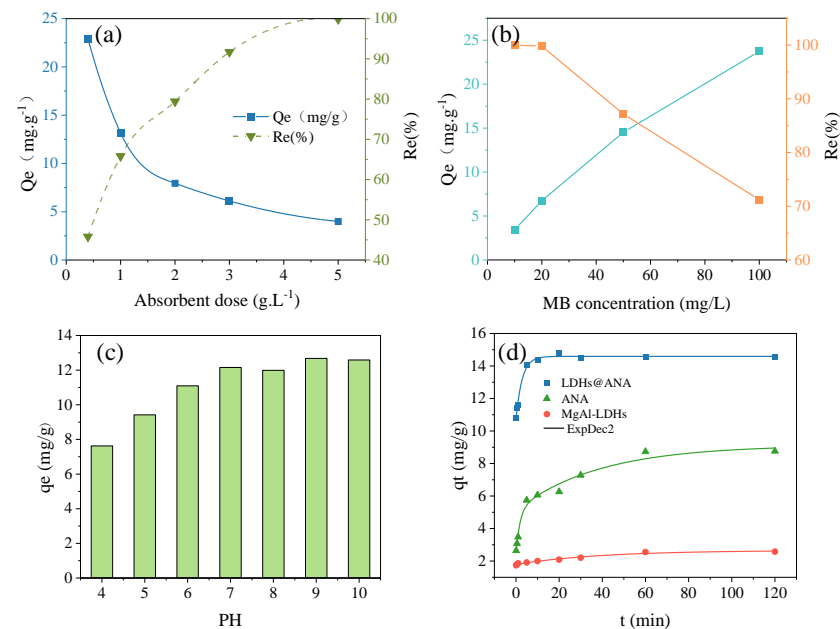


Figure 8. (a) Effects of adsorbent dose amount of LDHs@ANA composite on MB adsorption ($c(\text{MB}) = 20 \text{ mg/L}$, $T = 293 \text{ K}$, $\text{Ph} = 7.0$, $t = 1 \text{ h}$); (b) effects of initial MB concentration on the adsorption of MB by LDHs@ANA ($m/V = 3 \text{ g}\cdot\text{L}^{-1}$, $T = 293 \text{ K}$, $\text{Ph} = 7.0$, $t = 1 \text{ h}$); (c) effects of initial pH on MB adsorption by LDHs@ANA ($m/V = 3 \text{ g}\cdot\text{L}^{-1}$, $c(\text{MB}) = 50 \text{ mg/L}$, $T = 293 \text{ K}$, $t = 1 \text{ h}$); (d) Comparison of MB adsorption capacity by LDHs, ANA, and LDHs@ANA ($T = 293 \text{ K}$, $m/V = 3 \text{ g}\cdot\text{L}^{-1}$, $\text{pH} = 7.0$, $c(\text{MB}) = 50 \text{ mg}\cdot\text{L}^{-1}$, $t = 1 \text{ h}$, and the dashed lines were guided for the eye and represented an exponential behavior of ExpDec2).

3.3.2. Effect of Initial Concentration on MB Adsorption

Meanwhile, the initial concentration of MB had a significant effect on the Q_e and Re of LDHs@ANA. As shown in Figure 8b, as the initial concentration of MB solution increased, the adsorption capacity of the adsorbent increased, and at the same time, the adsorption efficiency decreased. Low concentrations of MB (<20 mg/L) could be completely adsorbed by LDHs@ANA, but when the concentration of MB increased to 100 mg/L, only 45.4% of MB was adsorbed. Since the number of adsorption sites of the adsorbent is certain, the removal efficiency of MB decreases with the increase of MB concentration.

3.3.3. Effect of PH on MB Adsorption

The effect of initial pH on the adsorption capacity of LDHs@ANA was explored (Figure 8c). As pH increased from 4 to 7, Q_e increased from 7.6 mg/g to 12.2 mg/g. Afterward, the pH increased from 7 to 10, and the adsorption capacity remained stable, indicating that alkaline conditions were beneficial for the adsorption of MB by LDHs@ANA. This may be due to the positive charge on the surface of LDHs@ANA and, thus, the strong electrostatic repulsion between LDHs@ANA and MB under acidic conditions. Due to electrostatic repulsion, the adsorption capacity of LDHs@ANA to cationic MB was reduced under acidic conditions. With the increase of pH, the deprotonation of functional groups makes LDHs@ANA negatively charged. The electrostatic attraction between the LDHs@ANA (negatively charged) and the MB (positively charged) led to an increase in the adsorption capacity.

3.3.4. Effect of Adsorbent Types on MB Adsorption

The adsorption effect of MgAl-LDHs, ANA, and LDHs@ANA composites on MB was studied, and the results are shown in Figure 8d. Compared with individual materials, the composite material significantly improved the adsorption capacity of MB. Specifically, the MB adsorption capacity of LDHs@ANA was 14.5 mg/L, which was significantly increased by 1.7 times and 5.6 times compared with ANA and MgAl-LDHs, respectively. The removal effect of LDHs@ANA composite on MB was much higher than that of the single adsorbent, which proved that the composite modification process was meaningful. On the one hand, under the action of electrostatic attraction, the positively charged LDH nanosheets were orderly attached to the negatively charged ANA surface, which was beneficial to reduce the disordered aggregation of LDH nanosheets, increasing the specific surface area. Further, the addition of urea during the hydrothermal reaction may have an effect on the ANA zeolite. The ammonia produced by the hydrolysis of urea has a leaching effect on Si in ANA, resulting in an increase in the net negative charge on the surface of the composite.

3.4. Adsorption Kinetics

Figure 9 shows the adsorption of LDHs@ANA on different initial concentrations of MB as a function of time. The experimental conditions were PH of 7.0, an adsorbent amount of $3 \text{ g} \cdot \text{L}^{-1}$, MB concentration of 20, 50, and 100 $\text{mg} \cdot \text{L}^{-1}$, respectively, an experimental temperature of 20 °C, and a reaction time of 120 min. The adsorption amount was increased with the increase of contact time until the adsorption equilibrium was approached. The adsorption capacity increased sharply in the first 10 min and increased slowly after 10 min. The maximum adsorption capacity increased with the increase of the initial concentration of MB. The initial concentration of MB increased from 20 mg/L to 100 mg/L, and the maximum adsorption capacity increased from 6.7 mg/L to 23.7 mg/L. Experimental data were fitted to pseudo-first-order and pseudo-second-order kinetic models. Linear plots of (t/q_t) against t for second-order models are shown in Figure S1. The regression coefficients (R^2) of second-order models exceeded 0.99 at different initial MB concentrations, which were all higher than first-order models (Figure S1). Therefore, the chemisorption was the rate-controlling step for MB adsorption by LDHs@ANA.

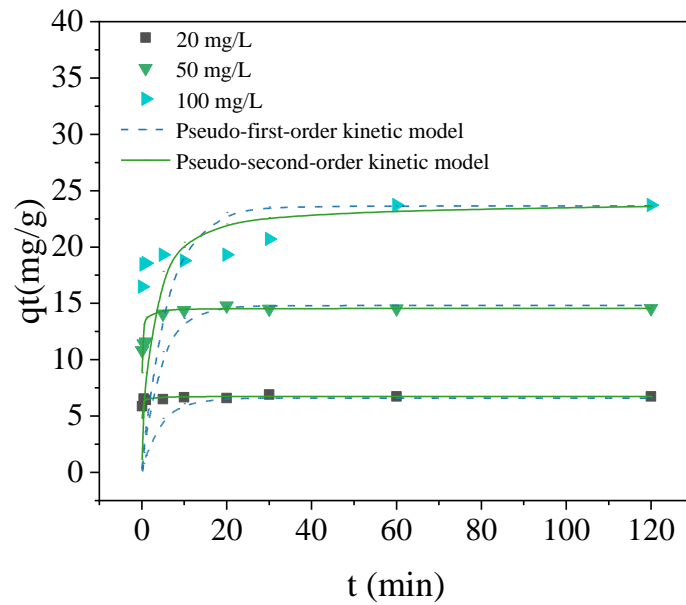


Figure 9. Adsorption kinetics fitting curves ($T = 293 \text{ K}$, $m/V = 3 \text{ g}\cdot\text{L}^{-1}$, and $\text{pH} = 7.0$).

3.5. Equilibrium Isotherm

The adsorption isotherms of MB on LDHs@ANA are shown in Figure 10, which indicates that the amount of adsorbed MB increases sharply with the increase of MB concentration in the initial stage and gradually tends to a plateau. As shown in Figure 10 and Table 3, the Langmuir, Freundlich, and Temkin adsorption isotherm models were used to fit and analyze the MB adsorption properties on the LDHs@ANA. According to the correlation coefficients (R^2), at all temperatures, the Langmuir model fits better than the Freundlich model and the Temkin model of the MB adsorption on the composite, followed by the Temkin model and Freundlich model (Table 4). Langmuir's theoretical maximum adsorption capacity of the MB adsorption on the composite at $20 \text{ }^\circ\text{C}$ reached 65.27 mg/g , indicating the excellent adsorption capacity of the composite on MB. Meanwhile, the maximum adsorption capacity decreased with increasing temperature, indicating that the adsorption process was exothermic.

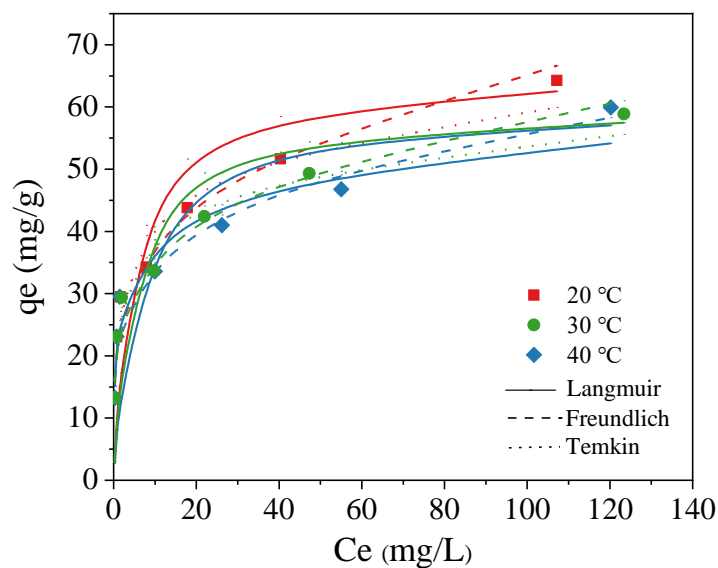


Figure 10. Langmuir, Freundlich, and Temkin adsorption isotherms fitting of LDHs@ANA composite for adsorption of MB.

Table 4. Isotherm calculation parameters of MB absorbed on the LDHs@ANA composite.

Models	Parameters	20 °C	30 °C	40 °C
Langmuir	Q_m	65.27	59.60	59.63
	K_L	0.2133	0.2210	0.1852
	R^2	0.9893	0.9919	0.9806
Freundlich	n	4.189	4.701	4.869
	K_F	21.83	21.92	21.81
	R^2	0.9517	0.9503	0.9097
Temkin	K_T	18.91	33.79	35.83
	b_T	308.61	365.16	376.36
	R^2	0.9684	0.9696	0.9351

4. Conclusions

In this study, we present a novel “SAD recovery for cationic dye wastewater treatment” approach to handle the problems of SAD resource consumption, low-cost LDHs@ANA composite synthesis, and cationic dye wastewater treatment all at once. Based on this strategy, the $Al(OH)_3$ extracted from SAD was used as an aluminum source to synthesize LDHs@ANA composite, which had more excellent adsorption capacity to MB than MgAl-LDHs and ANA alone. The composite consisted of spherical ANA particles uniformly covered with LDH nanosheets, which effectively avoided a large amount of aggregation between nanosheets and increased specific surface areas and pore volumes. The kinetic results indicated that the adsorption process conformed to the pseudo-second-order kinetic model, and the adsorption site was the main factor affecting the adsorption process. The equilibrium studies showed the adsorption process was exothermic, and the Langmuir model best fitted for the adsorption process, with q_{max} reaching 65.27 mg/g for MB. Overall, this work first transformed hazardous aluminum waste into LDHs@ANA for excellent cationic dye wastewater adsorption, which was meaningful to waste recovery and pollution control.

Supplementary Materials: The following supporting information can be downloaded at: <https://www.mdpi.com/article/10.3390/pr11041002/s1>, Figure S1: Plots of pseudo-second-order (a) model and pseudo-first-order (b); Table S1: Metallic contents of MgAl-LDHs, ANA, and LDHs@ANA.

Author Contributions: Writing—original draft, methodology, investigation, data curation, validation, formal analysis, investigation, writing, B.Z.; methodology, investigation, L.W.; review and editing, G.L.; conceptualization, supervision, Q.J. All authors have read and agreed to the published version of the manuscript.

Funding: This research received no external funding.

Institutional Review Board Statement: Not applicable.

Informed Consent Statement: Not applicable.

Data Availability Statement: The data that support the findings of this study are available from the corresponding author upon reasonable request.

Conflicts of Interest: The authors declare no conflict of interest.

References

- Mahinroosta, M.; Allahverdi, A. A promising green process for synthesis of high purity activated-alumina nanopowder from secondary aluminum dross. *J. Clean. Prod.* **2018**, *179*, 93–102. [CrossRef]
- Meshram, A.; Singh, K.K. Recovery of valuable products from hazardous aluminum dross: A review. *Resour. Conserv. Recycl.* **2018**, *130*, 95–108. [CrossRef]
- Mahinroosta, M.; Allahverdi, A. Hazardous aluminum dross characterization and recycling strategies: A critical review. *J. Environ. Manag.* **2018**, *223*, 452–468. [CrossRef]
- Hu, K.; Reed, D.; Robshaw, T.J.; Smith, R.M.; Ogden, M.D. Characterisation of aluminium black dross before and after stepwise salt-phase dissolution in non-aqueous solvents. *J. Hazard. Mater.* **2021**, *401*, 123351. [CrossRef] [PubMed]

5. David, E.; Kopac, J. Aluminum recovery as a product with high added value using aluminum hazardous waste. *J. Hazard. Mater.* **2013**, *261*, 316–324. [[CrossRef](#)]
6. He, L.; Shi, L.; Huang, Q.; Hayat, W.; Shang, Z.; Ma, T.; Wang, M.; Yao, W.; Huang, H.; Chen, R. Extraction of alumina from aluminum dross by a non-hazardous alkaline sintering process: Dissolution kinetics of alumina and silica from calcined materials. *Sci. Total Environ.* **2021**, *777*, 146123. [[CrossRef](#)]
7. Yang, Q.; Li, Q.; Zhang, G.; Shi, Q.; Feng, H. Investigation of leaching kinetics of aluminum extraction from secondary aluminum dross with use of hydrochloric acid. *Hydrometallurgy* **2019**, *187*, 158–167. [[CrossRef](#)]
8. Jiménez, A.; Rives, V.; Vicente, M.A.; Gil, A. A comparative study of acid and alkaline aluminum extraction valorization procedure for aluminum saline slags. *J. Environ. Chem. Eng.* **2022**, *10*, 107546. [[CrossRef](#)]
9. Khan, I.; Saeed, K.; Zekker, I.; Zhang, B.; Hendi, A.H.; Ahmad, A.; Ahmad, S.; Zada, N.; Ahmad, H.; Shah, L.A. Review on methylene blue: Its properties, uses, toxicity and photodegradation. *Water* **2022**, *14*, 242. [[CrossRef](#)]
10. Alghamdi, W.M.; El Mannoubi, I. Investigation of seeds and peels of *Citrullus colocynthis* as efficient natural adsorbent for methylene blue dye. *Processes* **2021**, *9*, 1279. [[CrossRef](#)]
11. Preetha, B.K.; Vishalakshi, B. Microwave assisted synthesis of karaya gum based montmorillonite nanocomposite: Characterisation, swelling and dye adsorption studies. *Int. J. Biol. Macromol.* **2020**, *154*, 739–750. [[CrossRef](#)] [[PubMed](#)]
12. EL-Mekkawi, D.M.; Ibrahim, F.A.; Selim, M.M. Removal of methylene blue from water using zeolites prepared from Egyptian kaolins collected from different sources. *J. Environ. Chem. Eng.* **2016**, *4*, 1417–1422. [[CrossRef](#)]
13. Lin, S.; Song, Z.; Che, G.; Ren, A.; Li, P.; Liu, C.; Zhang, J. Adsorption behavior of metal–organic frameworks for methylene blue from aqueous solution. *Microporous Mesoporous Mater.* **2014**, *193*, 27–34. [[CrossRef](#)]
14. Öden, M.K. Investigation of the success of physical and chemically modified process waste in heavy metal removal from synthetic wastewater. *J. Fac. Eng. Archit. Gaz.* **2020**, *35*, 39–49.
15. Dey, M.D.; Das, S.; Kumar, R.; Doley, R.; Bhattacharya, S.S.; Mukhopadhyay, R. Vermiremoval of methylene blue using *Eisenia fetida*: A potential strategy for bioremediation of synthetic dye-containing effluents. *Ecol. Eng.* **2017**, *106*, 200–208. [[CrossRef](#)]
16. Oden, M.K. Treatment of CNC industry wastewater by electrocoagulation technology: An application through response surface methodology. *Int. J. Environ. Anal. Chem.* **2020**, *100*, 1–19. [[CrossRef](#)]
17. Alpert, S.M.; Knappe, D.R.; Ducoste, J.J. Modeling the UV/hydrogen peroxide advanced oxidation process using computational fluid dynamics. *Water Res.* **2010**, *44*, 1797–1808. [[CrossRef](#)]
18. Katheresan, V.; Kannedo, J.; Lau, S.Y. Efficiency of various recent wastewater dye removal methods: A review. *J. Environ. Chem. Eng.* **2018**, *6*, 4676–4697. [[CrossRef](#)]
19. Rafatullah, M.; Sulaiman, O.; Hashim, R.; Ahmad, A. Adsorption of methylene blue on low-cost adsorbents: A review. *J. Hazard. Mater.* **2010**, *177*, 70–80. [[CrossRef](#)]
20. Vial, S.; Prevot, V.; Leroux, F.; Forano, C. Immobilization of urease in ZnAl layered double hydroxides by soft chemistry routes. *Microporous Mesoporous Mater.* **2008**, *107*, 190–201. [[CrossRef](#)]
21. Huang, Y.; Liu, C.; Rad, S.; He, H.; Qin, L. A comprehensive review of layered double hydroxide-based carbon composites as an environmental multifunctional material for wastewater treatment. *Processes* **2022**, *10*, 617. [[CrossRef](#)]
22. Goh, K.-H.; Lim, T.-T.; Dong, Z. Application of layered double hydroxides for removal of oxyanions: A review. *Water Res.* **2008**, *42*, 1343–1368. [[CrossRef](#)] [[PubMed](#)]
23. Lafi, R.; Charradi, K.; Djebbi, M.A.; Amara, A.B.H.; Hafiane, A. Adsorption study of Congo red dye from aqueous solution to Mg–Al-layered double hydroxide. *Adv. Powder. Technol.* **2016**, *27*, 232–237. [[CrossRef](#)]
24. Chen, D.; Li, Y.; Zhang, J.; Li, W.; Zhou, J.; Shao, L.; Qian, G. Efficient removal of dyes by a novel magnetic Fe₃O₄/ZnCr-layered double hydroxide adsorbent from heavy metal wastewater. *J. Hazard. Mater.* **2012**, *243*, 152–160. [[CrossRef](#)] [[PubMed](#)]
25. Wu, P.; Wu, T.; He, W.; Sun, L.; Li, Y.; Sun, D. Adsorption properties of dodecylsulfate-intercalated layered double hydroxide for various dyes in water. *Colloid Surf. A* **2013**, *436*, 726–731. [[CrossRef](#)]
26. Marangoni, R.; Bouhent, M.; Taviot-Guého, C.; Wypych, F.; Leroux, F. Zn₂Al layered double hydroxides intercalated and adsorbed with anionic blue dyes: A physico-chemical characterization. *J. Colloid Interface Sci.* **2009**, *333*, 120–127. [[CrossRef](#)] [[PubMed](#)]
27. Yang, Z.; Wang, F.; Zhang, C.; Zeng, G.; Tan, X.; Yu, Z.; Zhong, Y.; Wang, H.; Cui, F. Utilization of LDH-based materials as potential adsorbents and photocatalysts for the decontamination of dyes wastewater: A review. *RSC Adv.* **2016**, *6*, 79415–79436. [[CrossRef](#)]
28. Sharifi-Bonab, M.; Aber, S.; Salari, D.; Khodam, F. Synthesis of CoZnAl-layered double hydroxide/graphene oxide nanocomposite for the removal of methylene blue: Kinetic, thermodynamic, and isotherm studies. *Environ. Prog. Sustain. Energy* **2020**, *39*, e13316. [[CrossRef](#)]
29. Shi, Z.; Wang, Y.; Sun, S.; Zhang, C.; Wang, H. Removal of methylene blue from aqueous solution using Mg-Fe, Zn-Fe, Mn-Fe layered double hydroxide. *Water Sci. Technol.* **2020**, *81*, 2522–2532. [[CrossRef](#)]
30. Pérez-Botella, E.; Valencia, S.; Rey, F. Zeolites in Adsorption Processes: State of the Art and Future Prospects. *Chem. Rev.* **2022**, *122*, 17647–17695. [[CrossRef](#)]
31. Wang, H.; Xu, J.; Sheng, L. Purification mechanism of sewage from constructed wetlands with zeolite substrates: A review. *J. Clean. Prod.* **2020**, *258*, 120760. [[CrossRef](#)]
32. Kosinov, N.; Gascon, J.; Kapteijn, F.; Hensen, E.J. Recent developments in zeolite membranes for gas separation. *J. Membr. Sci.* **2016**, *499*, 65–79. [[CrossRef](#)]

33. Li, Y.; Wu, M.; Wu, J.; Wang, Y.; Zheng, Z.; Jiang, Z. Mechanistic insight and rapid co-adsorption of nitrogen pollution from micro-polluted water over MgAl-layered double hydroxide composite based on zeolite. *Sep. Purif. Technol.* **2022**, *297*, 121484. [[CrossRef](#)]
34. Wu, Y.; Song, L.; Shi, M.; Gu, C.; Zhang, J.; Lv, J.; Xuan, L. Ca/Fe-layered double hydroxide–zeolite composites for the control of phosphorus pollution in sediments: Performance, mechanisms, and microbial community response. *Chem. Eng. J.* **2022**, *450*, 138277. [[CrossRef](#)]
35. Mahinroosta, M.; Allahverdi, A. Enhanced alumina recovery from secondary aluminum dross for high purity nanostructured γ -alumina powder production: Kinetic study. *J. Environ. Manag.* **2018**, *212*, 278–291. [[CrossRef](#)]
36. Bhattacharyya, R.; Ray, S.K. Enhanced adsorption of synthetic dyes from aqueous solution by a semi-interpenetrating network hydrogel based on starch. *J. Ind. Eng. Chem.* **2014**, *20*, 3714–3725. [[CrossRef](#)]
37. Jiménez, A.; Misol, A.; Morato, Á.; Rives, V.; Vicente, M.A.; Gil, A. Synthesis of pollucite and analcime zeolites by recovering aluminum from a saline slag. *J. Clean. Prod.* **2021**, *297*, 126667. [[CrossRef](#)]
38. Murayama, N.; Maekawa, I.; Ushiro, H.; Miyoshi, T.; Shibata, J.; Valix, M. Synthesis of various layered double hydroxides using aluminum dross generated in aluminum recycling process. *Int. J. Miner. Process.* **2012**, *110*, 46–52. [[CrossRef](#)]
39. Sánchez-Hernández, R.; López-Delgado, A.; Padilla, I.; Galindo, R.; López-Andrés, S. One-step synthesis of NaP1, SOD and ANA from a hazardous aluminum solid waste. *Microporous Mesoporous Mater.* **2016**, *226*, 267–277. [[CrossRef](#)]
40. Sali, R.; Naik, L.; Mohan, S. Optical and Microstructural Changes in 5 (6)-Carboxyfluorescein Doped PVA. *J. Polym. Compos.* **2016**, *4*, 45–51.
41. Atta, A.; Jibril, B.; Aderemi, B.; Adefila, S. Preparation of analcime from local kaolin and rice husk ash. *Appl. Clay. Sci.* **2012**, *61*, 8–13. [[CrossRef](#)]
42. Šontevska, V.; Jovanovski, G.; Makreski, P.; Raškovska, A.; Šoptrajanov, B. Minerals from Macedonia. XXI. Vibrational spectroscopy as identificational tool for some phyllosilicate minerals. *Acta Chim. Slov.* **2008**, *55*, 757–766.
43. Thommes, M.; Kaneko, K.; Neimark, A.V.; Olivier, J.P.; Rodriguez-Reinoso, F.; Rouquerol, J.; Sing, K.S. Physisorption of gases, with special reference to the evaluation of surface area and pore size distribution (IUPAC Technical Report). *Pure Appl. Chem.* **2015**, *87*, 1051–1069. [[CrossRef](#)]
44. Zheng, M.; Wang, J.; Fu, D.; Ren, B.; Song, X.; Kan, K.; Zhang, X. Anchored growth of highly dispersed LDHs nanosheets on expanded graphite for fluoride adsorption properties and mechanism. *J. Hazard. Mater.* **2023**, *442*, 130068. [[CrossRef](#)] [[PubMed](#)]

Disclaimer/Publisher’s Note: The statements, opinions and data contained in all publications are solely those of the individual author(s) and contributor(s) and not of MDPI and/or the editor(s). MDPI and/or the editor(s) disclaim responsibility for any injury to people or property resulting from any ideas, methods, instructions or products referred to in the content.